GEODESY AND GEODYNAMICS 2016, VOL 7 NO 5, 323–328

Available online at www.sciencedirect.com

ScienceDirect

journal homepage: www.keaipublishing.com/en/journals/geog;
http://www.jgg09.com/jweb_ddcl_en/EN/volumn/home.shtml

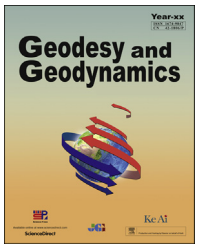

Coseismic and postseismic slip ruptures for 2015 Mw 6.4 Pishan earthquake constrained by static GPS solutions

Ping He[a,b,*], *Qi Wang*[a], *Kaihua Ding*[a,c], *Jie Li*[d], *Rong Zou*[a]

[a] *Hubei Subsurface Multi-scale Imaging Key Laboratory, Institute of Geophysics and Geomatics, China University of Geosciences, Wuhan, 430074, China*

[b] *Key Laboratory of Geospace Environment and Geodesy, Ministry of Education, Wuhan University, Wuhan, Hubei, 430079, China*

[c] *Faculty of Information Engineering, China University of Geosciences, Wuhan, 430074, China*

[d] *Earthquake Administration of Xinjiang Uygur Autonomous Region, Urumqi, 830011, China*

ARTICLE INFO

Article history:
Received 5 May 2016
Accepted 7 July 2016
Available online 30 July 2016

Keywords:
Pishan earthquake
Global Positioning System (GPS)
Coseismic deformation
Postseismic deformation
Model inversion

ABSTRACT

On 3 July 2015, a Mw 6.4 earthquake occurred on a blind fault struck Pishan, Xinjiang, China. By combining Crustal Movement Observation Network of China (CMONOC) and other Static Global Positioning System (GPS) sites surrounding Pishan region, it provides a rare chance for us to constrain the slip rupture for such a moderate event. The maximum displacement is up to 12 cm, 2 cm for coseismic and postseismic deformation, respectively, and both the deformation patterns show a same direction moving northeastward. With rectangular dislocation model, a magnitude of Mw6.48, Mw6.3 is calculated based on coseismic, postseismic deformation respectively. Our result indicates the western Kunlun range is still moving toward Tarim Basin followed by an obvious postseismic slip associated with this earthquake. To determine a more reasonable model for postseismic deformation, a longer GPS dataset will be needed.

How to cite this article: He P, et al., Coseismic and postseismic slip ruptures for 2015 Mw 6.4 Pishan earthquake constrained by static GPS solutions, Geodesy and Geodynamics (2016), 7, 323–328, http://dx.doi.org/10.1016/j.geog.2016.07.004.

* *Corresponding author*. Hubei Subsurface Multi-scale Imaging Key Laboratory, Institute of Geophysics and Geomatics, China University of Geosciences, Wuhan, 430074, China.
E-mail address: phe@cug.edu.cn (P. He).

Peer review under responsibility of Institute of Seismology, China Earthquake Administration.

Production and Hosting by Elsevier on behalf of KeAi

http://dx.doi.org/10.1016/j.geog.2016.07.004

1. Introduction

On 3 July 2015, at 01:07 UTC (local time at 09:07), an earthquake of Mw6.4, at a depth of 15 km, occurred at the north front of western Kunlun Mountain, about 133 km SE of Shache and 162 km WNW of Hetian. The epicenter, located only about 15 km southwest of Pishan city (USGS). In the first few days, after the main shock, there were thousands of aftershocks ($M \geq 2$) in the adjacent area; most of these aftershocks reveal an approximately fault strike direction (Fig. 1). According to the field geological investigation [1], no surface rupture was found which indicated the seismogenic fault was a blind fault beneath the surface ground. In spite of a moderate buried-rupture event, there were six people killed, hundreds of people injured, and more than 5000 housed destroyed [2]. In the past 40 years, only a couple of reverse-faulting earthquake ($M < 5.6$) occurred in this area, and none above M6.0 was recorded, implying that the seismicity is low [2,3]. This 2015 Pishan event significantly exceeded the expected seismic magnitude, which would lead a serious damage for the local constructions with their low antiseismic level. However, the detailed mechanisms of history earthquakes were unclear in consequence of few adequate geodetic observations in this area.

This 2015 Pishan earthquake just located between southwest boundary of the Tarim Basin and north front of western Kunlun range. According to the previous studies [3,6], the western Kunlun Mountain was one of the most important tectonic syntaxis of Tibetan Plateau, which extends along the range front, and there is a fast shortening of the upper crustal nappe since approximately 12 Ma has been well attested. There are three main fault segments including in this active area (Fig. 1), such as the left-slip Karakax Fault, an echelon left-lateral fault, and this western thrust system [3]. Geodetic observations indicate no more than 5 mm/yr coverage between western Tibet and Tarim [7]. Due to a thick desert covered, it is difficult to determine the rupture deformation for an earthquake through a field geological survey in this area [8]. Moreover, there is approximately 50 km region surrounding Pishan earthquake with no active Holocene faults found, according to the active tectonic map of China.

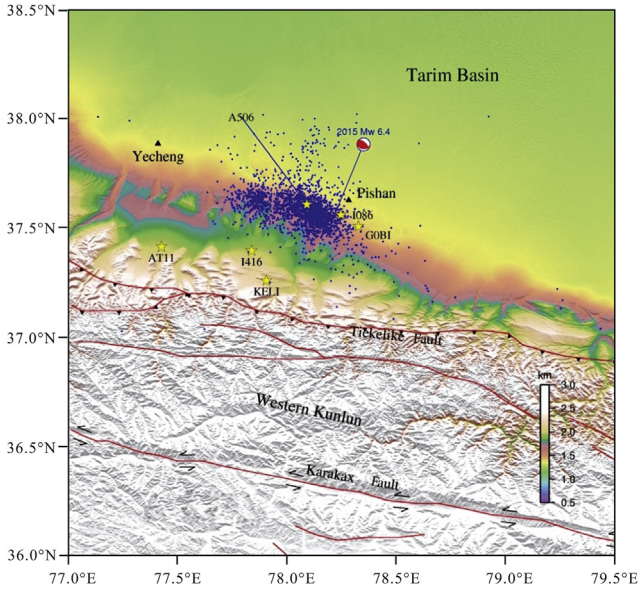

Fig. 1 – Active tectonics of the western Kunlun Mountain superimposed on a 3-arcsecond SRTM Digital Elevation Model (DEM). Red lines depict active faults [4]. Beachballs represent fault-plane solutions from the Harvard CMT catalogue, while the blue points show the aftershocks from the GCMT catalogue [5]. Yellow stars were the re-surveyed GPS sites.

As a rare chance to gain insights into the interaction between western Tibetan and Tarim, many studies focus on this event with different datasets, such as seismic reflection profile [1,8], Synthetic Aperture Radar Interferometry (InSAR) [9], and the Global Positioning System (GPS) [3]. All of them suggest that this event occurred at depth of 10–15 km on a buried fault except for slightly different dip angle. Seismic reflection profile is helpful to delineate the subsurface geometry of each fault segment in the fold belt, but which could not give a surface deformation and slip rupture produced by the seismogenic fault. InSAR is a powerful relative measurement tool with wide surface coverage which has been successfully used for many earthquakes, but atmospheric disturbance limits its precision at level of 1–2 cm [3,9]. In contrast to the above two measurements, GPS is an absolute measurement means which could provide 3-D surface displacement with high precision, especially in horizontal direction. Thanks to the resurvey GPS work of our group, it provides a chance for us to independently discuss both the coseismic and postseismic process for this event with only GPS observations.

In this article, both the coseismic and postseismic displacements associated with Pishan event are observed by "in-situ" static GPS measurements. Due to pre-earthquake surveys of these sites were carried out in different years by different agencies, the interseismic deformation must be considered before the coseismic deformation acquired. With another resurvey 5 months after the main shock, a postseismic deformation is estimated. Based on those GPS observations, both the coseismic and postseismic slip ruptures are constrained, and then potential seismic hazards in this area are discussed.

2. GPS data and processing

2.1. Data set

Usually, it is hard to find enough GPS sites in near-field to constrain the slip rupture for a moderate thrust event, because of its low surface deformation magnitude. It could be seen in Fig. 1 and Table 1 there are only two GPS sites in Crustal Movement Observation Network of China (CMONOC) near the epicenter of Pishan event. Fortunately, several groups implemented a GPS campaign based on the geodetic triangular point in Xinjiang Province around 2000 (Table 1), which makes it possible to improve the GPS site density and capture enough observations for this event in near-field region. There are totally 6 sites employed in this study,

Table 1 – Statistics of the GPS surveys (revised from He et al. [3]).

Site	Longitude (°)	Latitude (°)	First survey date	Epicentral distance (km)	CMONOC
			Pre-earthquake		Site (Y/N)
I086	78.246	37.559	June 15–18, 2013	13.7	Y
G0BI	78.327	37.506	June 15–18, 2000	16.1	N
A506	78.091	37.606	July 30–Aug.4, 1998	17.5	N
I416	77.838	37.394	June 23–26, 2013	28.9	Y
KELI	77.906	37.258	July 18–19, 2014	31.3	N
AT11	77.426	37.412	August 20–21, 1993	64.7	N

including three sites (I086, G0BI, and A506) near the epicenter within 20 km, two farther sites (I416 and KELI) about 30 km away, and a farmost site (AT11) about 65 km away.

GPS campaign was carried out two times by our survey group after the main shock, one is a month later, and the other is 4 months later. During these two times GPS field survey work, Trimble 5700 GPS receivers and Zephyr geodetic antennas were used to collect the data at 30 s sampling for 2–4 days, which is in order to guarantee an effective measurement time longer than 36 h at each site.

2.2. *Data processing*

The static GPS solutions are processed with GIPSY-OASIS-II (version 5.0) software developed by the Jet Propulsion Laboratory (JPL) [10]. In the processing, JPL's reanalyzed IGS08 orbit and clock products are adopted and absolute antenna phase center models for both GPS receiver and satellite antennas were refined [11]. To reduce tropospheric delay error, the Global Mapping Function (GMF) [12] tropospheric mapping function and the Global Pressure and Temperature (GPT) model [12] are utilized. In addition, the ocean tide model TPXO7.0 is used to correct the ocean tide loading. The more detailed processing could be referred to Ding et al. [13].

Combining the GPS data collected before and after the earthquake, we firstly deduced coseismic displacements caused by this event. Since the time of pre-earthquake survey is over decades for some sites, accumulated interseismic displacements could reach up a large value which could not be neglected in the coseismic displacement estimation. With several times surveys for two CMONOC sites (I086 and I416), an interseismic deformation rate in horizontal is estimated with 2.7 mm/yr N, 1.9 mm/yr E, and 2.7 mm/yr N, 2.0 mm/yr E respectively. Then the product of $t_{interval} \times v_{interseismic}$ is used to estimate the interseismic displacement for each site (where $t_{interval}$ is the time span, and $v_{interseismic}$ represents interseismic deformation rate). After that, an accurate coseismic displacement for each site is obtained [3]. However, this estimation probably contains a component of early postseismic deformation because our first time GPS survey was 1 month after the main shock. Only if a continuous real-time GPS station is in the near-field, otherwise it could not distinguish the early postseismic mixed in the coseismic deformation. Even though a little postseismic deformation mixed in GPS coseismic deformation, the coseismic deformation still greatly dominated in contrast to early postseismic deformation, which is the same appearance in an InSAR coseismic interferogram.

The second time GPS survey data is processed by the same strategy as the first one, and then a postseismic deformation acquired.

3. Coseismic and postseismic deformation

GPS coseismic offsets for each component listed in supporting material in He et al. [3], which are plotted in Fig. 2 in this paper. All the GPS sites in Fig. 2 show a same pattern moved northeastward. The maximum displacement is up to 12 cm in horizontal (4.4 cm in east–west and 10.8 cm in north–south) and 8.2 cm in vertical at A506, which is closest to the epicenter. In the southern part, a farther GPS site (KELI) shows about 2 cm displacement with no vertical displacement. Regarding of the AT11 site, it should be little deformation in theory with its long distance relative to the epicenter. While it shows a 4.57 cm offset in north direction. There are several possible factors analyzed for this abnormal signal as following: (1) data error derives from the pre-earthquake data; (2) gross error caused by instrument or surveyor; (3) a deformation caused by other unknown factor. Uncertainties reflect the dispersion of the position estimated over this time interval [13]. In addition, the uncertainty of horizontal component is only millimeter for most sites except AT11.

Compared with the GPS coseismic deformation, the postseismic deformation shown in Fig. 3 has a same pattern but a smaller magnitude. The postseismic deformation at site A506 could reach up 2–3 cm in this period, implying an obvious afterslip for Pishan event. This postseismic deformation is significantly different from the interseismic deformation and has a great significance to assess the potential hazard in this region. It is necessary to add the survey times in future to fully explore the various processes of postseismic motions.

4. Model for slip rupture

To further understand what role of the independent GPS data set could play in this event, a slip rupture inversion for both coseismic and postseismic deformation is completed by using the analytical solutions of a rectangular dislocation in a homogeneous, elastic half-space [14]. Here, we fix the fault geometry for the optimal fault plane provided by He et al. [3] and enable the fault length and width to be extended to 38 km along the strike and 30 km along the down-dip

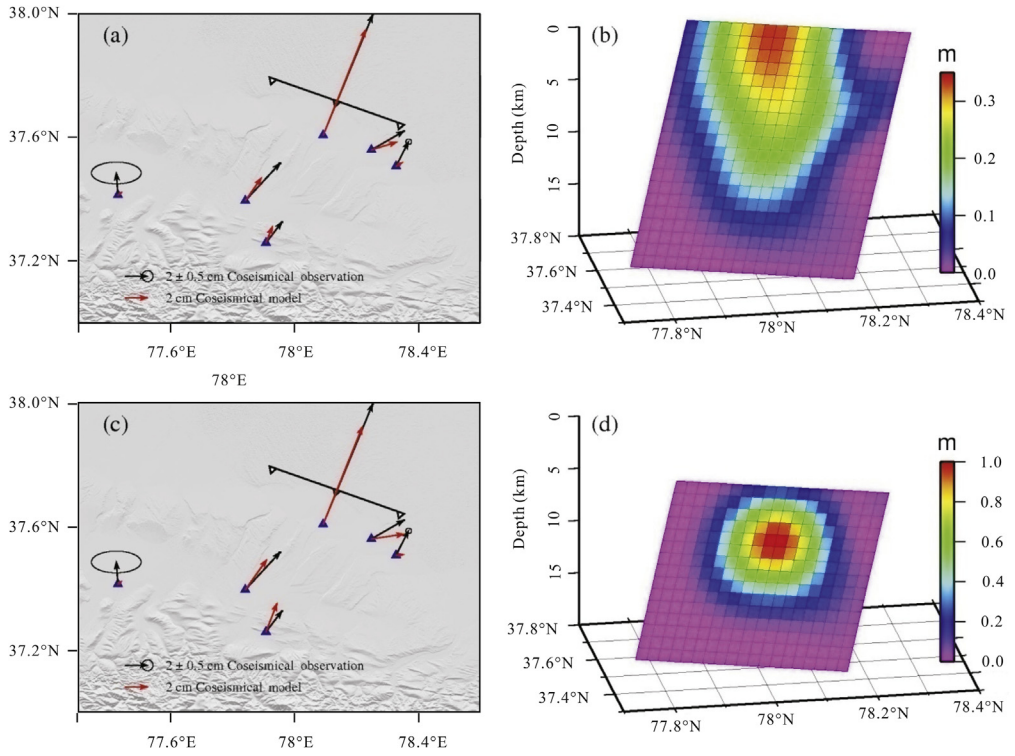

Fig. 2 – The coseismic geodetic observations and simulated displacements by distributed model. Black short line shows updip projection of the rupture at the surface. (a) Black and blue arrows correspond to GPS-derived horizontal displacement vectors and predicted ones (slip distribution without constrained), respectively. (b) Slip distribution of the Pishan earthquake without any constrained. (c) Black and blue arrows correspond to GPS-derived horizontal displacement vectors and predicted ones (slip distribution with shallow-slip constrained), respectively. (d) Slip distribution of the Pishan earthquake with shallow-slip constrained.

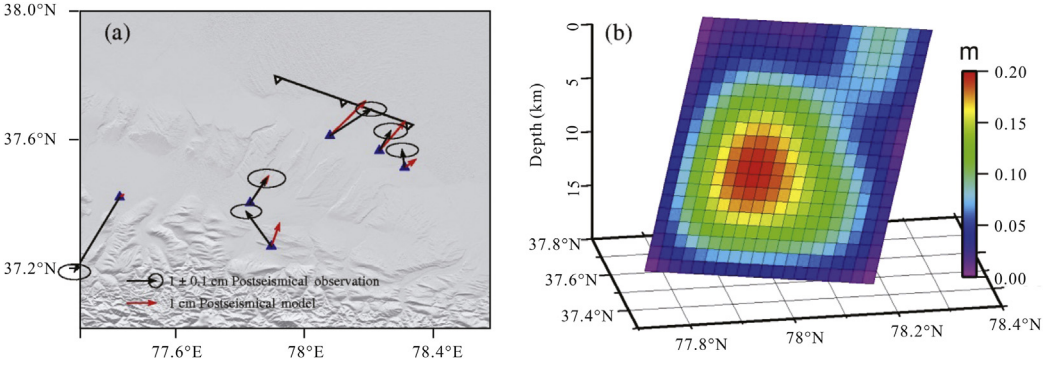

Fig. 3 – The postseismic geodetic observations and simulated displacements by distributed model. Black short line shows updip projection of the rupture at the surface. (a) Black and blue arrows correspond to GPS-derived horizontal displacement vectors and predicted ones, respectively. (b) Afterslip distribution of the Pishan earthquake without any constrained.

direction, and then discrete it into 95 patches with a size of 2 km by 2 km. After that, a non-negative linear least-squares procedure [15] is used to solve slip vectors (dip- and strike-slip components) of these patches.

4.1. *Model of coseismic deformation*

Based on the GPS data, a preferred coseismic slip distribution is shown in Fig. 2(b) with no shallow-slip

constrained. The slip rupture is concentrated above 5 km depth with only one slip patch, and the maximum slip is 0.35 m located at the surface. The distributed slip model yields a geodetic moment of 4.81×10^{18} N·m equivalently a Mw6.39, slightly smaller than that inferred from the InSAR + GPS inversion [3]. However, the main slip should rupture beneath the surface for with the previous studies [1,3,8,9], and this slip distribution without depth constrained is not consistent with a blind fault event. The main reason maybe GPS is more sensitive than other data for shallow information in slip inversion.

The focal mechanism solutions from the United States Geological Survey (USGS), GCMT, and China Earthquake Networks Center (CENC) indicate that the 2015 Pishan earthquake occurred beneath 10 km depth. In addition, there was no surface rupture found by field surface geology. With the above prior information, a model inversion with shallow-slip constrained is carried out. After the slip confined to beneath 5 km, a slip distribution is inversed with the same fault geometry shown in Fig. 2 (d). The slip rupture is concentrated as a disc with 4 km by 4 km size at depth of 10–12 km, and the maximum slip is 0.93 m. The distributed slip model yields a geodetic moment of 6.42×10^{18} N·m equivalently a Mw6.48, larger than that inferred from the unconstrained slip model and close to that of CENC.

4.2. *Model of postseismic deformation*

According to the time-dependent earthquake rupture theory [16,17], postseismic deformation yields to a logarithmic decay model and it could last a various period ranges from several weeks [18] to hundreds of years [19]. High density of postseismic deformation survey both in time and space is the key to get a perfect result, but mostly it is hard to meet this requirement. However, the postseismic deformation in this paper still has a great significance to reflect the postseismic tectonic activity for this medium blind fault event.

A simple afterslip model was estimated based on the postseismic deformation in section 3 using elastic dislocation theory as in the coseismic case. The same fault geometry was assumed as for the coseismic model. Afterslip distribution inverted in Fig. 3 shows a large afterslip located at depth of 5–14 km, and extended almost entirely the whole fault plane. The maximum afterslip in the model is up to 0.2 m, which is about one-fifth that of coseismic slip. The afterslip has released a geodetic moment of 4.03×10^{18} N·m corresponds to a Mw6.3 sub-event.

5. Discussion and conclusion

Static GPS data independently capture coseismic and postseismic deformation caused by the Pishan earthquake provided a rare observations for such a moderate earthquake. As an independent high-precision (<5 mm) survey technique, GPS has been widely used in many earthquakes research, especially for large earthquake such as 2008 Wenchuan [20], 2010 Tohoku-Oki [21], and 2015 Gorkha Nepal [22]. However, there are only a few moderate earthquakes have been constrained with only GPS survey [23,24]. Because the deformation scale of moderate earthquake is usually within a radius of 10–20 km, which is much smaller than the interval length of two GPS sites in network in most places of the world. Thanks to the GPS sites shared by other agencies, the density of GPS network has greatly improved by integrating CMONOC and other GPS sites for Pishan earthquake.

As the first major event occurred along the northwestern edge of Tibetan Plateau, GPS coseismic and postseismic deformation in this article will be helpful to assess the tectonic activity and potential geologic hazards in this region. This Pishan event has triggered approximately 10 cm coseismic deformation and approximately 2 cm postseismic deformation which can be seen clearly in Figs. 2(a) and 3(a). Regarding of the pattern of coseismic and postseismic deformation, it shows a same pattern moved northeastward, which indicated the western Kunlun Mountain is still moving toward Tarim Basin and the afterslip is ongoing. It is a good agreement with seismic reflection profiles results given by Lu et al. [8].

With a depth constrained, coseismic slip distribution fits well with GPS coseismic deformation. All the previous studies [1,3,8,9] confirmed that Pishan earthquake occurred on a blind fault at depth of 10 km, and the maximum slip is 0.5–1.0 m. Fig. 2(d) reveals a similar slip rupture at 10–14 km depth, which strongly support GPS sites in this article have an independent capacity to constrain the slip rupture for this event. Compare with the two slip patches given by He et al. [1] and Wen et al. [9], the upper slip patch could not be identified in this article. In the perspective of detailed constraint, a longer GPS observations are needed. However, GPS data provided an independent observation for Pishan event to some extent, which will improve the sensitivity to determine the shallow slip rupture [25].

It is surprising and interesting that the postseismic slip rupture release a moment equal the main shock. If the structure of lithosphere is conducive to the stress release in this study area, it will reduce the potential earthquake risk. Postseismic slip rupture in Fig. 3(b) displays the afterslip originates from a surrounding extension of the coseismic rupture on the fault plane. Yet it is hard to distinguish whether the postseismic deformation caused by afterslip or viscoelastic relaxation mechanisms with the limited data. A longer data set will be required to study the most probable model for postseismic deformation.

Acknowledgments

This work is supported by National Natural Science Foundation of China (41304014, 41204001, 41274037 and 41431069), National 863 Project of China (2013AA122501), China postdoctoral science foundation (2015M57228), the Basic Fund of Hubei Subsurface Multi-scale Imaging Key Laboratory, Institute of Geophysics and Geomatics, China University of Geosciences, Wuhan (SMIL-2015-01), the Fundamental Research Funds for National Universities (CUGL150810), China Scholarship Council (201506415072), and the Basic Research Fund of Key Laboratory of Geospace Environment and Geodesy,

Ministry of Education of China (13-02-11 and 14-01-01). Ping He is a visiting research scientist in University of Michigan (UM) supported by the State Scholarship Fund of China.

REFERENCES

[1] Li T, Chen J, Fang L, Chen Z, Thompson JA, Jia C. The 2015 Mw 6.4 Pishan earthquake: seismic hazards of an active blind Wedge thrust system at the western Kunlun range front, northwest Tibetan Plateau. Seismol Res Lett 2016;87(3):1–8.

[2] Feng G, Li Z, Xu B, Shan X, Zhang L, Zhu J. Coseismic deformation of the 2015 Mw 6.4 Pishan, China, earthquake estimated from Sentinel-1A and ALOS2 data. Seismol Res Lett 2016;87(4):800–6.

[3] He P, Wang Q, Ding K, Wang M, Qiao X, Li J, et al. Source model of the 2015 Mw 6.4 Pishan earthquake constrained by interferometric synthetic aperture radar and GPS: insight into blind rupture in the western Kunlun Shan. Geophys Res Lett 2016;43:1511–9.

[4] Taylor M, Yin A. Active structures of the Himalayan-Tibetan orogen and their relationships to earthquake distribution, contemporary strain field, and Cenozoic volcanism. Geosphere 2009;5(3):199–214. http://dx.doi.org/10.1130/GES00217.1.

[5] Ekström G, Nettles M, Dziewoński A. The global CMT project 2004–2010: centroid-moment tensors for 13,017 earthquakes. Phys Earth Planet Inter 2012;200–201:1–9. http://dx.doi.org/10.1016/j.pepi.2012.04.002.

[6] Jiang X, Li Z, Li H. Uplift of the West Kunlun Range, northern Tibetan Plateau, dominated by brittle thickening of the upper crust. Geology 2013;41(4):439–42.

[7] Wang Q, Zhang PZ, Freymueller JT, Bilham R, Larson KM, Lai XA, et al. Present-day crustal deformation in China constrained by global positioning system measurements. Science 2001;294(5542):574–7.

[8] Lu R, Xu X, He D, Liu B, Tan X, Wang X. Coseismic and blind fault of the 2015 Pishan Mw 6.5 earthquake: implications for the sedimentary-tectonic framework of the western Kunlun Mountains, northern Tibetan Plateau. Tectonics 2016;35:1–9.

[9] Wen Y, Xu C, Liu Y, Jiang G. Deformation and source Parameters of the 2015 Mw 6.5 earthquake in Pishan, western China, from Sentinel-1A and ALOS-2 data. Remote Sens 2016;8(2):134.

[10] Zumberge JF, Heflin MB, Jefferson DC, Watkins MM, Webb FH. Precise point positioning for the efficient and robust analysis of GPS data from large networks. J Geophys Res Solid Earth 1997;102(B3):5005–17.

[11] Schmid R, Steigenberger P, Gendt G, Ge M, Rothacher M. Generation of a consistent absolute phase-center correction model for GPS receiver and satellite antennas. J Geodesy 2007;81(12):781–98.

[12] Böehm J, Heinkelmann R, Schuh H. Short note: a global model of pressure and temperature for geodetic applications. J Geodesy 2007;81(10):679–83.

[13] Ding K, Freymueller JT, Wang Q, Zou R. Coseismic and early postseismic deformation of the 5 January 2013 Mw 7.5 Craig earthquake from static and kinematic GPS solutions. Bull Seismol Soc Am 2015;105(2B):1153–64.

[14] Okada Y. Surface deformation due to shear and tensile faults in a half-space. Bull Seismol Soc Am 1985;75(4):1135–54.

[15] Wang L, Wang R, Roth F, Enescu B, Hainzl S, Ergintav S. Afterslip and viscoelastic relaxation following the 1999 M 7.4 Izmit earthquake from GPS measurements. Geophys J Int 2009;178(3):1220–37.

[16] Reid HF, State Earthquake Investigation Commission. The California earthquake of April 18, 1906: Report of the State Earthquake Investigation Commission. The mechanics of the earthquake, vol. 2. Carnegie Inst. of Washington; 1910. p. 1–192.

[17] Das S, Scholz CH. Theory of time-dependent rupture in the earth. J Geophys Res Solid Earth 1981;86(B7):6039–51.

[18] Bürgmann R, Kogan MG, Levin VE, Scholz CH, King RW, Steblov GM. Rapid aseismic moment release following the 5 December, 1997 Kronotsky, Kamchatka, earthquake. Geophys Res Lett 2001;28(7):1331–4.

[19] Gourmelen N, Amelung F. Postseismic mantle relaxation in the central Nevada seismic belt. Science 2005;310(5753):1473–6.

[20] Wang Q, Qiao X, Lan Q, Freymuller J, Yang S, Xu C, et al. Rupture of deep faults in the 2008 Wenchuan earthquake and uplift of the Longmen Shan. Nat Geosci 2011;4(9):634–40. http://dx.doi.org/10.1038/ngeo1210.

[21] Ozawa S, Nishimura T, Suito H, Kobayashi T, Tobita M, Imakiire T. Coseismic and postseismic slip of the 2011 magnitude-9 Tohoku-Oki earthquake. Nature 2011;475(7356):373–6.

[22] Galetzka J, Melgar D, Genrich JF, Geng J, Owen S, Lindsey EO, et al. Slip pulse and resonance of the Kathmandu basin during the 2015 Gorkha earthquake. Nepal Sci 2015;349(6252):1091–5.

[23] Anzidei M, Boschi E, Cannelli V, Devoti R, Esposito A, Galvani A, et al. Coseismic deformation of the destructive April 6, 2009 L'Aquila earthquake (central Italy) from GPS data. Geophys Res Lett 2009;36(17).

[24] Jiang Z, Wang M, Wang Y, Wu Y, Che S, Shen ZK, et al. GPS constrained coseismic source and slip distribution of the 2013 Mw6. 6 Lushan, China, earthquake and its tectonic implications. Geophys Res Lett 2014;41(2):407–13.

[25] Yue H, Lay T, Rivera L, An C, Vigny C, Tong X, et al. Localized fault slip to the trench in the 2010 Maule, Chile Mw = 8.8 earthquake from joint inversion of high-rate GPS, teleseismic body waves, InSAR, campaign GPS, and tsunami observations. J Geophys Res Solid Earth 2014;119(10):7786–804.

Ping He, Ph.D., Lecturer. His research interests include theory and algorithm of InSAR and GPS and its application, especially for crust deformation and its dynamical model.